

Ultrafast anisotropic protein quake propagation after CO photodissociation in myoglobin

Levin U. L. Brinkmann^{a,b} and Jochen S. Hub^{a,b,1}

^aInstitute for Microbiology and Genetics, Georg-August University Göttingen, 37077 Goettingen, Germany; and ^bGöttingen Center for Molecular Biosciences, Georg-August University Göttingen, 37077 Goettingen, Germany

Edited by Michael Levitt, Stanford University School of Medicine, Stanford, CA, and approved July 21, 2016 (received for review March 3, 2016)

“Protein quake” denotes the dissipation of excess energy across a protein, in response to a local perturbation such as the breaking of a chemical bond or the absorption of a photon. Femtosecond time-resolved small- and wide-angle X-ray scattering (TR-SWAXS) is capable of tracking such ultrafast protein dynamics. However, because the structural interpretation of the experiments is complicated, a molecular picture of protein quakes has remained elusive. In addition, new questions arose from recent TR-SWAXS data that were interpreted as underdamped oscillations of an entire protein, thus challenging the long-standing concept of overdamped global protein dynamics. Based on molecular-dynamics simulations, we present a detailed molecular movie of the protein quake after carbon monoxide (CO) photodissociation in myoglobin. The simulations suggest that the protein quake is characterized by a single pressure peak that propagates anisotropically within 500 fs across the protein and further into the solvent. By computing TR-SWAXS patterns from the simulations, we could interpret features in the reciprocal-space SWAXS signals as specific real-space dynamics, such as CO displacement and pressure wave propagation. Remarkably, we found that the small-angle data primarily detect modulations of the solvent density but not oscillations of the bare protein, thereby reconciling recent TR-SWAXS experiments with the notion of overdamped global protein dynamics.

time-resolved SAXS/WAXS | free-electron laser | molecular dynamics

Functional protein dynamics occur on various timescales, ranging from tens of femtoseconds for bond breaking, up to milliseconds and seconds for large-scale conformational transitions or protein folding. Observing and explaining such transitions, if possible in a time-resolved manner, has remained a central goal of molecular biophysics. A popular model system used to study proteins dynamics has been the 18-kDa protein myoglobin (Mb), the protein of first known tertiary structure (1). Mb contains an iron-porphyrin heme group that reversibly binds small gas molecules such as molecular oxygen (O₂) or carbon monoxide (CO). Mb is abundant in the muscle tissue of vertebrates, where it plays an important role in the transport and storage of O₂ and in the biochemistry of nitric oxide (2, 3).

Because the CO-iron bonds in a Mb ensemble can be coherently photolysed with a laser flash within only 50 fs (4), a range of time-resolved techniques has been applied to probe various aspects of the structural dynamics after CO photodissociation, such as energy dissipation, CO dynamics, or heme doming (5–15). Three-dimensional movies of Mb conformational transitions were derived by means of time-resolved crystallography, which recently reached subpicosecond time resolution (16–19). These experimental studies were complemented by several pioneering molecular-dynamics (MD) simulations that revealed the Mb dynamics with atomic detail, with some focus on heat dissipation, vibrational dynamics, as well as ligand migration (20–28).

Time-resolved small- and wide-angle X-ray scattering (TR-SAXS, TR-WAXS, TR-SWAXS) is an emerging technique used to track conformational transitions in solution. The method has been applied to follow chemical reactions of small molecules (29–31) as well as structural dynamics of photoactive proteins (32–41).

Thanks to the advent of X-ray free-electron lasers, TR-SWAXS experiments have reached subpicosecond time resolution, thus detecting the ultrafast dynamics of proteins. Hence, TR-SWAXS is able to track the ultrafast dissipation of energy in proteins triggered by a local perturbation, due to, for instance, the breaking of a chemical bond or the deposition of energy upon photon absorption (42, 43). Such dynamics of energy dissipation have been referred to as “protein quakes” (44). These new experiments provide valuable insight into the ultrafast dynamics of proteins in solution, but they also raised new questions. Oscillations in the small-angle data detected by recent TR-SWAXS experiments were interpreted as underdamped oscillations of the entire protein (43), thus challenging the long-standing notion of overdamped large-scale protein dynamics (45, 46). However, the structural interpretation of SWAXS patterns has remained problematic mainly for two reasons. First, SWAXS patterns contain only few independent data points (for Mb, ~14 data points at a maximum momentum transfer of 1 Å⁻¹) (47), whereas proteins contain orders of magnitude more degrees of freedom. Second, scattering contributions from the hydration layer complicate the interpretation of the patterns; as shown here, solvent effects may even dominate the signals. These complications preclude a straightforward fitting of structural models against TR-SWAXS data without significant risk of overfitting.

MD simulations have been used to interpret experimental data of low information content via back-calculating experimental signals from the simulation frames. To apply this strategy to TR-WAXS data, we recently developed an algorithm for the calculation of isotropic and anisotropic TR-SWAXS patterns from explicit-solvent MD simulations, which we here used to study the ultrafast dynamics after CO photodissociation in Mb. The calculations are fully based on explicit-solvent MD, thus accounting for scattering contributions from density modulations in the hydration layer (48, 49).

Significance

Scattering in solution conducted at X-ray free-electron lasers in principle provides a probe for the ultrafast dynamics of proteins. However, extracting useful structural information from the experimental signals remains a major challenge. Here, we used molecular-dynamics simulations to model the ultrafast “quake-like” dissipation of energy in myoglobin. The simulations provide a detailed atomistic movie of the protein quake, and they help to translate solution scattering signals into functional protein dynamics. Remarkably, we further find that accounting for solvent dynamics is crucial to avoid misinterpretation of time-resolved solution scattering data.

Author contributions: L.U.L.B. and J.S.H. designed research, performed research, analyzed data, and wrote the paper.

The authors declare no conflict of interest.

This article is a PNAS Direct Submission.

¹To whom correspondence should be addressed. Email: jhub@gwdg.de.

This article contains supporting information online at www.pnas.org/lookup/suppl/doi:10.1073/pnas.1603539113/-DCSupplemental.

Results

Time-Resolved WAXS Patterns. The CO dissociation was modeled classically, as done previously (ref. 28 and references therein), by instantaneously switching the force field from the CO bound to the dissociated state. Assuming an excitation laser of 532-nm wavelength and a reaction enthalpy of $96.5 \text{ kJ}\cdot\text{mol}^{-1}$, we added the appropriate amount of kinetic energy to the nitrogen atoms of the porphyrin ring to ensure that the total amount of dissipated energy agrees with experimental conditions (*SI Materials and Methods*). The dissociation kinetics was similar to previous studies, characterized by cooling of the CO within 300 fs due to collisions with protein atoms, and a cooling of the heme within 1–2 ps, followed by slower relaxations (Fig. S1) (5, 10).

TR-WAXS experiments report the difference in scattering intensity of the system before and after CO photodissociation, as a function of the time delay Δt after excitation. We computed 2D difference patterns from $\sim 10,000$ 100-ps simulations of CO photodissociation, combined with $\sim 10,000$ simulations of Mb in the ground state (Fig. 1). Fig. 2A and Fig. S2 present typical TR-WAXS patterns, and the azimuthal average over the detector $I_{aa}(q, \Delta t)$ is shown in Fig. 2B. Here, the momentum transfer is defined as $q = 4\pi\lambda^{-1} \sin(\theta)$, where 2θ is the scattering angle and λ is the wavelength of the X-ray beam. Because heme is a circular absorber, Mb in which the heme plane is oriented parallel to the excitation laser polarization is excited with higher probability,

leading to anisotropic ensembles of excited and ground-state Mb (50). Hence, additional structural details are given by the anisotropy $\Delta I_{\text{aniso}}(q)$ of the TR-WAXS patterns (48, 51, 52), here computed as the difference between the horizontal and vertical cuts on the detector (Fig. 2C and Fig. S3). These reciprocal-space signals are rationalized in real space in Fig. 2F and Movie S1, visualizing the CO movements and the protein quake propagation in terms of electron density differences after photodissociation, averaged over $\sim 10,000$ simulations. In addition, Fig. 2G quantifies the protein quake in terms of time-resolved center-of-mass displacement of a number of residues and α -helices.

Within 100 fs after photodissociation, the CO was fully displaced along the heme normal, which manifests in $I_{aa}(q, \Delta t)$ as a permanent minimum at $q = 0.75 \text{ \AA}^{-1}$ (Fig. 2B, green bar). Indeed, the signals lack this minimum when the CO atoms are omitted from the WAXS calculations (Fig. 2E and Fig. S4). Hence, the ultrafast appearance of the $q = 0.75 \text{ \AA}^{-1}$ minimum, which is compatible with recent TR-WAXS experiments (43), primarily reflects the CO displacement, complementing previous studies that interpreted features in the WAXS patterns mainly as fingerprints for tertiary conformational transitions (34, 43, 53). Simultaneously, a transient signal at 0.28 \AA^{-1} built up within 250 fs (Fig. 2B, orange bar, and D), which is much less dependent on the CO atoms. Because the time courses of the 0.28 \AA^{-1} signal and of the protein quake visible in Movie S1 are similar, we suggest that the 0.28 \AA^{-1} signal is the main fingerprint of the protein quake in reciprocal space. Because this signal had diminished at 500 fs, it might have been invisible to recent TR-WAXS experiments by Levantino et al. (43) with a time resolution of ~ 500 fs. In line with reports by Ihee and coworkers (51), our simulations predict highly anisotropic patterns, reflecting that the CO displacement as well as the follow-up protein dynamics occur in an oriented manner with respect to the heme plane (Fig. 2C and F).

On longer timescales, picosecond dynamics manifest as a separate well at $q = 0.35 \text{ \AA}^{-1}$ appearing after $\Delta t > 1$ ps, as also observed in experimental data (34, 41, 43, 53). This peak was found to be less prominent in simulation compared with experiments, possibly because the applied MD force field did not reproduce the doming of the heme structure (Fig. 2D; see also *SI Discussion* for simulations with an alternative force field). However, the overall reasonable agreement to experimental TR-WAXS data suggests that the dynamics in the simulations resemble the experimental conditions.

As visualized in Fig. 2F and Movie S1, the pressure wave (or protein quake) propagated anisotropically, whereas the most rapid propagation occurred perpendicular to the heme plane: within 100 fs, Leu-29 and the proximal His-93 were perturbed by the dissociated CO and by the displaced iron, respectively, thus shifted away from the heme plane (Fig. 2G). Until a time delay of 150 fs, these perturbations further propagated across the backbones of helices B and F into Ile-30 and Ala-94, triggering damped oscillations with a period between 300 and 450 fs, compatible with recent findings from serial femtosecond crystallography (19). At 500 fs, nearly the complete helices B and F were perturbed. In contrast, in the direction parallel to the heme plane, the propagation occurred with a significant delay. Within 100 fs, the side chain of Phe-43 shifted, as also observed by crystallography (19), but it took ~ 300 fs until this perturbation had propagated into the backbone of helix C. In helix E, Val-68 and His-64 were likewise perturbed by the dissociating CO within 100 fs, but this perturbation hardly propagated into the backbone of helix E, even until 1 ps. In addition, the CO moved between 150 and 500 fs from the pocket between Leu-29, Leu-32, Phe-43, His-64 further toward Ile-107 and into the distal pocket, rationalizing why Ile-107 was perturbed with delay of ~ 500 fs (Fig. 2G, magenta) (19). The relaxation after the initial pressure wave occurred also in an asynchronous manner. For instance, the

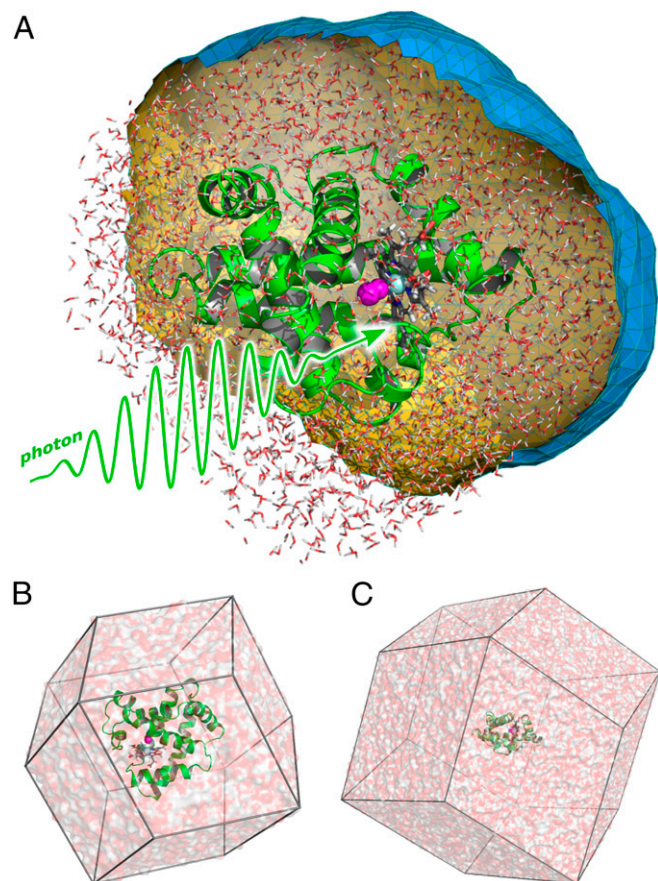


Fig. 1. (A) Molecular representation of myoglobin (Mb). The backbone trace is shown as green cartoon, the heme as gray sticks, CO as magenta spheres, and iron as light blue sphere. A spatial envelope, here at a distance of 6 Å from all protein atoms, is shown as blue/orange surface. Water atoms (white/red sticks) inside the envelope contribute to the SWAXS calculations. (B) Typical small and (C) large simulation system of Mb, used to compute WAXS and SAXS patterns, respectively.

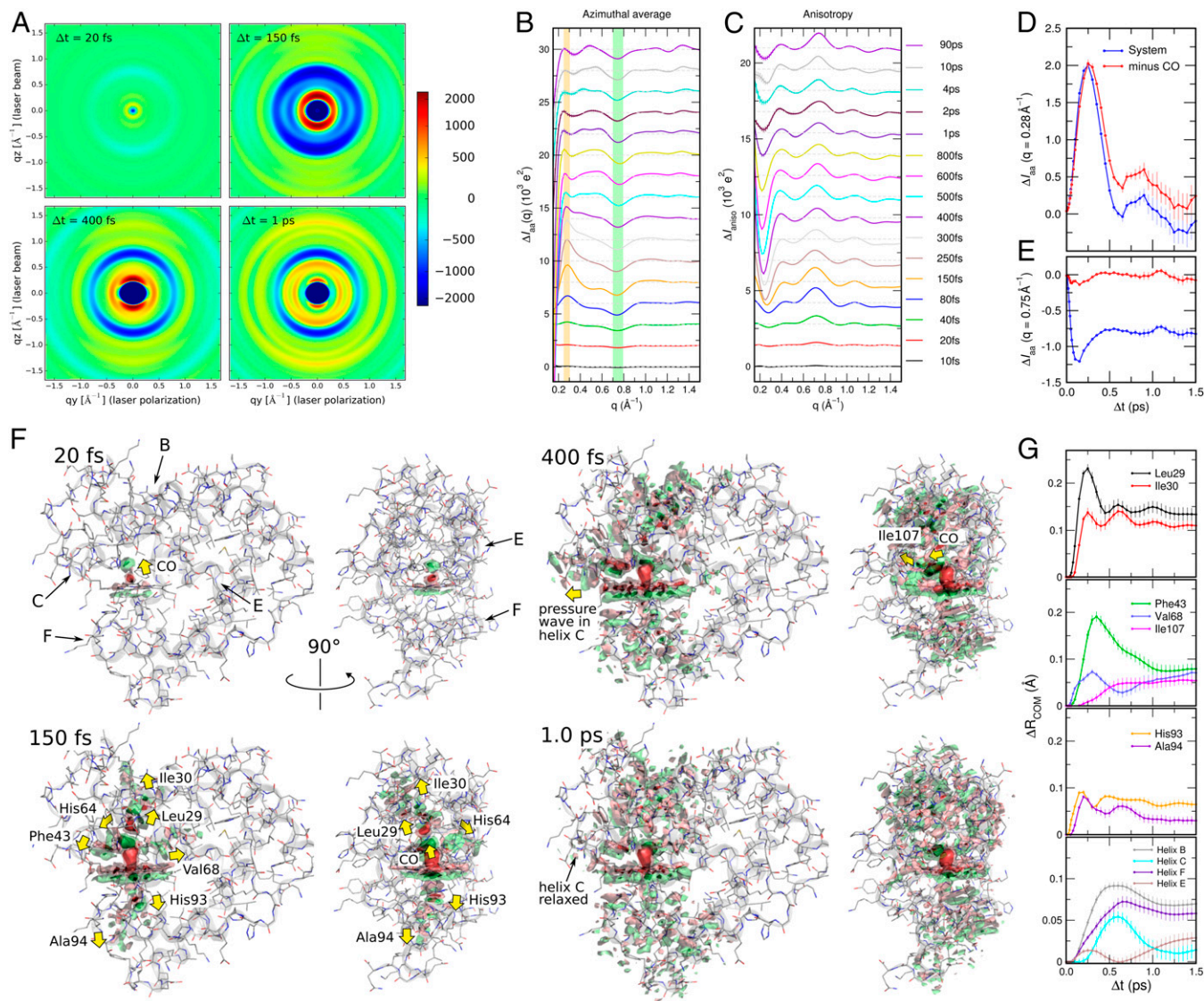


Fig. 2. (A) Time-resolved anisotropic WAXS patterns of Mb in units of e^2 . (B) Azimuthal average over the detector for time delays between 10 fs and 90 ps, and (C) anisotropy of the WAXS patterns, taken as the difference between the horizontal and vertical cuts in A. Curves at $\Delta t > 10$ fs were offset for clarity. (D and E) Azimuthally averaged intensities at 0.28 and 0.75 \AA^{-1} versus time delay (B, orange and green bars), computed from the whole system (blue), or by omitting the CO atoms (red). (F) Isosurfaces of the electron density difference maps at 20 fs, 150 fs, 400 fs, and 1.0 ps after photodissociation. Green and red surfaces indicate increased and reduced density, respectively. Opaque green and red surfaces: $\pm 400 \text{ e}\cdot\text{nm}^{-3}$; transparent green and red surfaces: $\pm 100 \text{ e}\cdot\text{nm}^{-3}$. Additional time delays are visualized in [Movie S1](#). (G) Time-resolved center-of-mass displacement of a number of residues (top three panels) and α -helices (bottom panel), with respect to their position at $\Delta t = 0$, as indicated in the legends. The density differences in F and curves in G illustrate the propagation of the protein quake.

displacements of Leu-29 had relaxed at 450 fs, of Phe-43 side chain at 650 fs, and of the backbone of helix C at 1 ps. Taken together, the excess energy propagated as a pressure wave within ~ 500 fs across the protein in a highly anisotropic and asynchronous manner, and the wave is echoed in the TR-WAXS pattern as a transient anisotropic peak at $q = 0.28 \text{ \AA}^{-1}$.

Time-Resolved SAXS Patterns. It is well established that the density of the hydration layer of proteins may differ from the density of bulk water, thus contributing to the overall density contrast detected by SAXS experiments (54). Accordingly, we observed that the pressure wave triggered by CO dissociation propagated across the hydration layer and further into bulk water, with significant fingerprints in the SAXS patterns. To account for such effects, we conducted 10,000 additional simulations of Mb in a larger simulation box (Fig. 1C). The time-resolved change of the

solvent density averaged from these simulations showed that the pressure wave had reached the protein surface after 300 fs, and subsequently propagated into the solvent with the speed of sound (Fig. 3B).

Guided by these solvent density curves, we first computed the SAXS patterns including explicit solvent contributions up to a distance of 17 \AA from the protein, as solvent contributions from larger distances added systematic errors due to tiny drifts in the solvent density. The apparent change in the radius of gyration $\Delta R_g^{\text{Guin}}(\Delta t)$ and total protein volume $\Delta V^{\text{Guin}}(\Delta t)$ were computed by fitting the Guinier approximation to the buffer-subtracted SAXS curves, $\ln[I(q)/I(0)] = -(qR_g^{\text{Guin}})^2/3$, thus accounting for scattering contributions from the hydration layer (*SI Materials and Methods*). The results are presented in Fig. 3C and D as black curves, which resemble the curves fitted by Levantino et al.

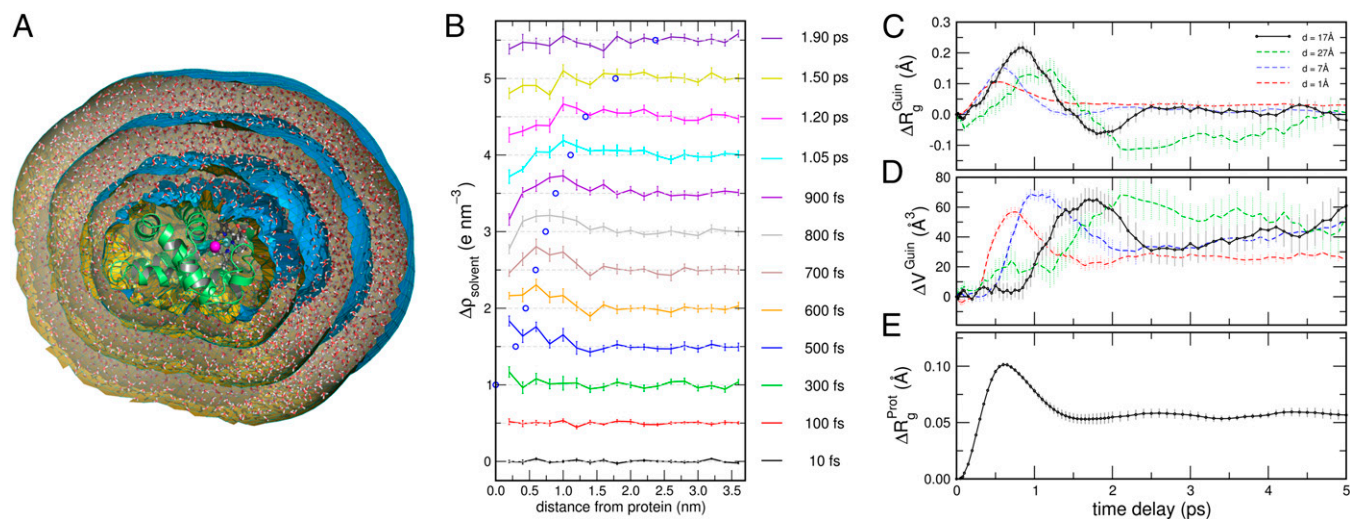


Fig. 3. Analysis of the small-angle scattering data. (A) Mb (green cartoon) and explicit water (sticks) enclosed by envelopes with distance of 1, 7, 17, and 27 Å (blue surfaces). (B) Time-resolved change of the solvent density after CO photodissociation versus distance from the protein, demonstrating the propagation of a pressure wave across the hydration layer within ~ 2 ps after CO photodissociation. Blue circles: Peak propagation expected from the speed of sound (1.48 nm/ps). (C) Time evolution of the radius of gyration after CO photodissociation $\Delta R_g^{\text{Guin}}(t)$ extracted from the Guinier analysis, thus taking hydration layer contributions into account. Color coding indicates calculations from different distance d of the envelope from the protein (see legend). (D) Volume of the protein taken from the forward intensity $I(q=0)$. (E) Increase of radius of gyration of the bare protein ΔR_g^{Prot} , ignoring any solvent effects.

(43) against experimental TR-SAXS data. In particular, ΔR_g^{Guin} exhibited an oscillatory shape with a maximum after ~ 1 ps, whereas the increase in ΔV^{Guin} is delayed. However, the magnitude of the modulations were smaller in the simulations, and a second shallow oscillatory peak observed in experiments was not reproduced by our calculations.

Strikingly, the radius of gyration of the bare protein ΔR_g^{Prot} , computed purely from the protein atomic coordinates, exhibited a highly different temporal course compared with ΔR_g^{Guin} (Fig. 3E and Fig. S5). Namely, ΔR_g^{Prot} is characterized by an ultrafast increase within ~ 650 fs up to only one-half the value observed in ΔR_g^{Guin} , followed by an overdamped decay to the new equilibrium value. Similar dynamics were found from the center-of-mass displacements of the α -helices (Fig. 2G and Fig. S6). This apparent discrepancy between ΔR_g^{Guin} and ΔR_g^{Prot} can be rationalized by computing ΔR_g^{Guin} taking an increasing thickness of solvent into account (Fig. 3C, black and colored curves; illustrated in Fig. 3A and Fig. S7), yielding ΔR_g^{Guin} curves that differ purely due to modulations of the solvent density. As expected, taking nearly no solvent into account (Fig. 3C, red) leads to an ΔR_g^{Guin} progression that is identical to the ΔR_g^{Prot} computed from the solute atoms, with a maximum at ~ 650 fs. When increasing the thickness of the included hydration layer, the maximum in ΔR_g^{Guin} increases and shifts to longer Δt , reflecting a delayed escape of the pressure wave from the envelope. Likewise, the time course of ΔV^{Guin} strongly depends on the thickness of solvent taken into account, demonstrating that ΔV^{Guin} is also dominated by solvent contributions (Fig. 3D, black and colored curves). This analysis shows that TR-SAXS experiments with subpicosecond time resolution can detect the propagation of the pressure wave into the solvent. The dynamics of the bare protein, however, contribute only partly to the SAXS signal and may therefore be hidden by signals from the solvent density modulations.

Discussion

MD simulations provide atomistic insight into the time evolution of protein quakes, that is, the ultrafast dissipation of excess energy in response to a local perturbations, such as the breaking of a chemical bond. By comparing the simulations to TR-SAXS, TR-WAXS, and time-resolved crystallographic data, we validated that the dynamics in simulation resemble the experimental conditions.

We showed that the protein quake and the CO displacement leave characteristic fingerprints in the anisotropic scattering patterns, thus allowing us to interpret features in the reciprocal-space signals in terms of specific real-space conformational dynamics.

Our simulations suggest that the protein quake triggered by CO photodissociation is characterized by a single pressure wave that propagates in a highly anisotropic and asynchronous manner across the protein matrix. The pressure wave propagated perpendicular to the heme plane, in the direction of the initial momenta of the CO and iron just after bond breaking. Notably, the computed difference electron density maps reported here for the femtosecond-to-picosecond time range (Fig. 2F) resemble the anisotropic distribution of experimental features in a difference electron density map for a crystallized dimeric hemoglobin at 100-ps time delay (55). This may be taken as an indication that ultrafast dynamics may underlie transitions into long-living states. The perturbation parallel to the heme plane occurred with delay, and parts of the protein were not perturbed even picoseconds after the trigger. The quake did not propagate along the backbone trace, as envisioned in the pioneering work by Ansari et al. (44). Instead, the momentum of the primary perturbation as well as modulations in local packing and compressibility emerge as the main determinants for protein quake propagation. After ~ 300 fs, the pressure peak started to propagate across the hydration layer. The pressure pattern in the hydration shell did not exhibit any indication for underdamped oscillations but instead resembles the patterns observed for explosive blast waves (56), that is, a pressure peak was followed by a pressure minimum at ~ 1 ps, which relaxed back to the equilibrium value at ~ 2 ps. Taken together, protein quakes are a striking example for the coupling between solvent and protein dynamics (57).

The theory of sound suggests that only a small fraction of the energy propagating with the protein quake is reflected at the protein/water interface. The ratio of the reflected energy may be estimated by the reflection coefficient $R = [(Z_w - Z_p)/(Z_w + Z_p)]^2$, where Z_w and Z_p denote the mechanical impedances of water and protein, respectively (58). The impedance is defined as $Z = \rho_m c$, where ρ_m is the mass density and c is the speed of sound. Assuming that the speed of sound in the protein is 2.3 nm/ps (59), one obtains a reflection coefficient of only $\sim 15\%$, which seems to

be too low to allow underdamped oscillations of the protein (*SI Materials and Methods*). To further test the influence of the solvent on Mb dynamics, we carried out additional CO dissociation simulations with the protein in vacuum at constant energy conditions, thus imposing a reflection coefficient of $R = 100\%$. In contrast to Mb in water, Mb in vacuum showed clear underdamped oscillations with a period ~ 1.8 ps (Fig. S8). Hence, the internal friction of Mb is small and would per se allow underdamped oscillations. For Mb in solvent, however, because the impedances of protein and water are similar, the protein quake energy dissipates into the solvent, leading to overdamped protein dynamics.

TR-SAXS and TR-WAXS experiments have recently become available with unprecedented time resolution, opening new opportunities to follow ultrafast protein dynamics such as protein quakes (42, 43). Because the interpretation of the reciprocal-space signals is notoriously difficult, these new experiments raised new questions. Levantino et al. (43) observed underdamped oscillations in the ΔR_g^{Guin} and ΔV^{Guin} after CO photodissociation in Mb, which were interpreted as underdamped oscillations of the protein. This interpretation was surprising because large-scale collective motions of proteins in water were assumed to be overdamped and subject to low Reynolds numbers (46). Our simulations offer an alternative interpretation of the TR-SAXS data. We found that ΔR_g^{Guin} and ΔV^{Guin} are dominated by modulations of the solvent density. Hence, the small-angle data of Mb report on protein dynamics only up to ~ 500 fs, after which the signals are dominated by the propagation of the pressure wave into the solvent. These findings highlight the importance of accurately modeling the solvent effects when interpreting solution scattering data. The dynamics of the radius of gyration of the bare protein (R_g^{Prot}) was characterized by a ballistic expansion up to ~ 650 fs followed by an overdamped relaxation up to 1.7 ps, thus compatible with the long-standing concept of overdamped global protein dynamics. To further validate these conclusions, we modeled the absorption of multiple photons, thereby (i) increasing the total amount of dissipated energy and (ii) modulating the energy fractions dissipated via the CO and via the heme (Fig. S9). The additional energy led to a larger increase of R_g^{Prot} followed by additional picosecond relaxation, but the protein dynamics did not change qualitatively.

Remaining slight discrepancies in the WAXS patterns around 0.4 \AA^{-1} suggest that the energy dissipated via the CO compared with the iron were not fully reproduced by the classical force fields. We also tested the effect of switching to the force field suggested

by Karplus and coworkers (60) upon photodissociation, which explicitly models the displacement of the iron with respect to the heme plane in the five-coordinated state. As expected, this force field reproduced the doming of the heme, but the discrepancy in the WAXS patterns increased, suggesting that more expensive quantum chemical methods might be required to model the dynamics of iron displacement and heme doming accurately (12, 13, 19). Additional discrepancies might originate from the fact that, in contrast to experimental conditions, our TR-WAXS calculations are assuming a low excitation laser intensity (48). Regarding the analysis of ΔR_g^{Guin} and ΔV^{Guin} , we note that the calculations are accurate up to ~ 2 ps after photodissociation, after which the pressure wave leaves the envelope. At longer delay times, when the pressure wave has propagated further into bulk water, the explicit-solvent calculations would require a very large envelope, thereby suffering from systematic errors due to tiny drifts in the overall solvent density (Fig. 3 C and D, green curves). Hence, SAXS calculations for long time delays might benefit from continuum models in future studies.

To conclude, our simulations suggest that the protein quake in Mb is characterized by a single pressure peak that propagates anisotropically and asynchronously through the protein matrix, followed by an overdamped relaxation. The pressure wave manifests (i) as a transient anisotropic peak in the WAXS patterns in the subpicosecond range, and (ii) as picosecond modulations of ΔR_g^{Guin} and ΔV^{Guin} as the wave propagates across the hydration layer into bulk solvent. The simulations thus provide atomic insight into ultrafast dynamics of proteins, and they aid the interpretation of scattering experiments conducted at free-electron lasers.

Materials and Methods

The initial structure of horse heart Mb was taken from the Protein Data Bank [PDB ID code 1DWR (61)]. All simulations were conducted in explicit solvent, if not stated otherwise. Simulations used to compute the WAXS patterns and the modulations in electron density (Fig. 2) contained 9,205 explicit-solvent water molecules (Fig. 1B). Simulations used to compute SAXS patterns contained 70,188 explicit-solvent water molecules (Fig. 1C). SAXS/WAXS patterns were computed following the explicit-solvent calculations we introduced recently (48, 49). The protein was described by the CHARMM22* force field (62). The simulations were conducted with the Gromacs software (63). More details are provided in *SI Materials and Methods* (64–74).

ACKNOWLEDGMENTS. We thank K. Atkovska and N. Awasthi for critically reading the manuscript. This work was supported by Deutsche Forschungsgemeinschaft Grant HU 1971-1/1.

- Kendrew JC, et al. (1958) A three-dimensional model of the myoglobin molecule obtained by x-ray analysis. *Nature* 181(4610):662–666.
- Wittenberg BA, Wittenberg JB (1989) Transport of oxygen in muscle. *Annu Rev Physiol* 51(1):857–878.
- Flögel U, Merx MW, Gödecke A, Decking UK, Schrader J (2001) Myoglobin: A scavenger of bioactive NO. *Proc Natl Acad Sci USA* 98(2):735–740.
- Petrich JW, Poyart C, Martin JL (1988) Photophysics and reactivity of heme proteins: A femtosecond absorption study of hemoglobin, myoglobin, and protoheme. *Biochemistry* 27(11):4049–4060.
- Mizutani Y, Kitagawa T (1997) Direct observation of cooling of heme upon photodissociation of carbonmonooxy myoglobin. *Science* 278(5337):443–446.
- Genberg L, Heisel F, McLendon G, Miller RD (1987) Vibrational energy relaxation processes in heme proteins: Model systems of vibrational energy dispersion in disordered systems. *J Phys Chem* 91(22):5521–5524.
- Lim M, Jackson TA, Anfirud PA (1993) Nonexponential protein relaxation: Dynamics of conformational change in myoglobin. *Proc Natl Acad Sci USA* 90(12):5801–5804.
- Ansari A, Jones CM, Henry ER, Hofrichter J, Eaton WA (1994) Conformational relaxation and ligand binding in myoglobin. *Biochemistry* 33(17):5128–5145.
- Austin RH, Beeson KW, Eisenstein L, Frauenfelder H, Gunsalus IC (1975) Dynamics of ligand binding to myoglobin. *Biochemistry* 14(24):5355–5373.
- Anfirud PA, Han C, Hochstrasser RM (1989) Direct observations of ligand dynamics in hemoglobin by subpicosecond infrared spectroscopy. *Proc Natl Acad Sci USA* 86(21):8387–8391.
- Lim M, Jackson TA, Anfirud PA (1997) Ultrafast rotation and trapping of carbon monoxide dissociated from myoglobin. *Nat Struct Biol* 4(3):209–214.
- Schlichting I, Berendzen J, Phillips GN, Jr, Sweet RM (1994) Crystal structure of photolysed carbonmonooxy-myoglobin. *Nature* 371(6500):808–812.
- Franzen S, Bohn B, Poyart C, Martin JL (1995) Evidence for sub-picosecond heme doming in hemoglobin and myoglobin: A time-resolved resonance Raman comparison of carbonmonooxy and deoxy species. *Biochemistry* 34(4):1224–1237.
- Genberg L, Richard L, McLendon G, Miller RD (1991) Direct observation of global protein motion in hemoglobin and myoglobin on picosecond time scales. *Science* 251(4997):1051–1054.
- Sato A, Gao Y, Kitagawa T, Mizutani Y (2007) Primary protein response after ligand photodissociation in carbonmonooxy myoglobin. *Proc Natl Acad Sci USA* 104(23):9627–9632.
- Srajer V, et al. (1996) Photolysis of the carbon monoxide complex of myoglobin: Nanosecond time-resolved crystallography. *Science* 274(5293):1726–1729.
- Srajer V, et al. (2001) Protein conformational relaxation and ligand migration in myoglobin: A nanosecond to millisecond molecular movie from time-resolved Laue X-ray diffraction. *Biochemistry* 40(46):13802–13815.
- Schotte F, et al. (2003) Watching a protein as it functions with 150-ps time-resolved x-ray crystallography. *Science* 300(5627):1944–1947.
- Barends TR, et al. (2015) Direct observation of ultrafast collective motions in CO myoglobin upon ligand dissociation. *Science* 350(6259):445–450.
- Henry ER, Eaton WA, Hochstrasser RM (1986) Molecular dynamics simulations of cooling in laser-excited heme proteins. *Proc Natl Acad Sci USA* 83(23):8982–8986.
- Case DA, Karplus M (1979) Dynamics of ligand binding to heme proteins. *J Mol Biol* 132(3):343–368.
- Ma J, Huo S, Straub JE (1997) Molecular dynamics simulation study of the B-states of solvated carbon monoxymyoglobin. *J Am Chem Soc* 119(10):2541–2551.
- Kottalam J, Case DA (1988) Dynamics of ligand escape from the heme pocket of myoglobin. *J Am Chem Soc* 110(23):7690–7697.

24. Elber R, Karplus M (1990) Enhanced sampling in molecular dynamics: Use of the time-dependent Hartree approximation for a simulation of carbon monoxide diffusion through myoglobin. *J Am Chem Soc* 112(25):9161–9175.
25. Straub JE, Karplus M (1991) Molecular dynamics study of the photodissociation of carbon monoxide from myoglobin: Ligand dynamics in the first 10 ps. *Chem Phys* 158(2-3):221–248.
26. Schaad O, Zhou HX, Szabo A, Eaton WA, Henry ER (1993) Simulation of the kinetics of ligand binding to a protein by molecular dynamics: Geminate rebinding of nitric oxide to myoglobin. *Proc Natl Acad Sci USA* 90(20):9547–9551.
27. Vitkup D, Petsko GA, Karplus M (1997) A comparison between molecular dynamics and X-ray results for dissociated CO in myoglobin. *Nat Struct Biol* 4(3):202–208.
28. Hummer G, Schotte F, Anfinrud PA (2004) Unveiling functional protein motions with picosecond x-ray crystallography and molecular dynamics simulations. *Proc Natl Acad Sci USA* 101(43):15330–15334.
29. Neutze R, et al. (2001) Visualizing photochemical dynamics in solution through picosecond x-ray scattering. *Phys Rev Lett* 87(19):195508.
30. Davidsson J, et al. (2005) Structural determination of a transient isomer of CH₂I₂ by picosecond X-ray diffraction. *Phys Rev Lett* 94(24):245503.
31. Ihee H, et al. (2005) Ultrafast x-ray diffraction of transient molecular structures in solution. *Science* 309(5738):1223–1227.
32. Cammarata M, et al. (2008) Tracking the structural dynamics of proteins in solution using time-resolved wide-angle X-ray scattering. *Nat Methods* 5(10):881–886.
33. Ahn S, Kim KH, Kim Y, Kim J, Ihee H (2009) Protein tertiary structural changes visualized by time-resolved X-ray solution scattering. *J Phys Chem B* 113(40):13131–13133.
34. Cho HS, et al. (2010) Protein structural dynamics in solution unveiled via 100-ps time-resolved x-ray scattering. *Proc Natl Acad Sci USA* 107(16):7281–7286.
35. Ramachandran PL, et al. (2011) The short-lived signaling state of the photoactive yellow protein photoreceptor revealed by combined structural probes. *J Am Chem Soc* 133(24):9395–9404.
36. Kim KH, et al. (2012) Direct observation of cooperative protein structural dynamics of homodimeric hemoglobin from 100 ps to 10 ms with pump-probe X-ray solution scattering. *J Am Chem Soc* 134(16):7001–7008.
37. Andersson M, Vincent J, van der Spoel D, Davidsson J, Neutze R (2008) A proposed time-resolved X-ray scattering approach to track local and global conformational changes in membrane transport proteins. *Structure* 16(1):21–28.
38. Andersson M, et al. (2009) Structural dynamics of light-driven proton pumps. *Structure* 17(9):1265–1275.
39. Malmerberg E, et al. (2011) Time-resolved WAXS reveals accelerated conformational changes in iodoretinal-substituted proteorhodopsin. *Biophys J* 101(6):1345–1353.
40. Westenhoff S, et al. (2010) Rapid readout detector captures protein time-resolved WAXS. *Nat Methods* 7(10):775–776.
41. Oang KY, et al. (2014) Sub-100-ps structural dynamics of horse heart myoglobin probed by time-resolved X-ray solution scattering. *Chem Phys* 422:137–142.
42. Arnlund D, et al. (2014) Visualizing a protein quake with time-resolved X-ray scattering at a free-electron laser. *Nat Methods* 11(9):923–926.
43. Levantino M, et al. (2015) Ultrafast myoglobin structural dynamics observed with an X-ray free-electron laser. *Nat Commun* 6:6772.
44. Ansari A, et al. (1985) Protein states and proteinquakes. *Proc Natl Acad Sci USA* 82(15):5000–5004.
45. Parak F, Knapp EW (1984) A consistent picture of protein dynamics. *Proc Natl Acad Sci USA* 81(22):7088–7092.
46. McCammon JA, Harvey SC (1988) *Dynamics of Proteins and Nucleic Acids* (Cambridge Univ Press, Cambridge, UK).
47. Putnam CD, Hammel M, Hura GL, Tainer JA (2007) X-ray solution scattering (SAXS) combined with crystallography and computation: Defining accurate macromolecular structures, conformations and assemblies in solution. *Q Rev Biophys* 40(3):191–285.
48. Brinkmann LUL, Hub JS (2015) Anisotropic time-resolved solution X-ray scattering patterns from explicit-solvent molecular dynamics. *J Chem Phys* 143(10):104108.
49. Chen PC, Hub JS (2014) Validating solution ensembles from molecular dynamics simulation by wide-angle X-ray scattering data. *Biophys J* 107(2):435–447.
50. Ansari A, Jones CM, Henry ER, Hofrichter J, Eaton WA (1993) Photoselection in polarized photolysis experiments on heme proteins. *Biophys J* 64(3):852–868.
51. Kim J, et al. (2011) Anisotropic picosecond x-ray solution scattering from photoselectively aligned protein molecules. *J Phys Chem Lett* 2(5):350–356.
52. Cho HS, Schotte F, Dashdorj N, Kyndt J, Anfinrud PA (2013) Probing anisotropic structure changes in proteins with picosecond time-resolved small-angle X-ray scattering. *J Phys Chem B* 117(49):15825–15832.
53. Kim KH, et al. (2011) Direct observation of myoglobin structural dynamics from 100 picoseconds to 1 microsecond with picosecond X-ray solution scattering. *Chem Commun (Camb)* 47(1):289–291.
54. Merzel F, Smith JC (2002) Is the first hydration shell of lysozyme of higher density than bulk water? *Proc Natl Acad Sci USA* 99(8):5378–5383.
55. Ren Z, Šrajcar V, Knapp JE, Royer WE, Jr (2012) Cooperative macromolecular device revealed by meta-analysis of static and time-resolved structures. *Proc Natl Acad Sci USA* 109(1):107–112.
56. Kinney GF, Graham KJ (1885) *Explosive Shocks in Air* (Springer, Berlin), 2nd Ed.
57. Brooks CL, 3rd, Karplus M (1989) Solvent effects on protein motion and protein effects on solvent motion. Dynamics of the active site region of lysozyme. *J Mol Biol* 208(1):159–181.
58. Landau LD, Lifshitz EM (1989) *Fluid Mechanics* (Pergamon Press, Oxford).
59. Yu X, Leitner DM (2003) Vibrational energy transfer and heat conduction in a protein. *J Phys Chem B* 107(7):1698–1707.
60. Meuwly M, Becker OM, Stote R, Karplus M (2002) NO rebinding to myoglobin: A reactive molecular dynamics study. *Biophys Chem* 98(1-2):183–207.
61. Chu K, et al. (2000) Structure of a ligand-binding intermediate in wild-type carbon-monoxide myoglobin. *Nature* 403(6772):921–923.
62. Piana S, Lindorff-Larsen K, Shaw DE (2011) How robust are protein folding simulations with respect to force field parameterization? *Biophys J* 100(9):L47–L49.
63. Pronk S, et al. (2013) GROMACS 4.5: A high-throughput and highly parallel open source molecular simulation toolkit. *Bioinformatics* 29(7):845–854.
64. Jorgensen WL, Chandrasekhar J, Madura JD, Impey RW, Klein ML (1983) Comparison of simple potential functions for simulating liquid water. *J Chem Phys* 79(2):926–935.
65. Horn HW, et al. (2004) Development of an improved four-site water model for biomolecular simulations: TIP4P-Ew. *J Chem Phys* 120(20):9665–9678.
66. Essmann U, et al. (1995) A smooth particle mesh Ewald potential. *J Chem Phys* 103(19):8577–8592.
67. Miyamoto S, Kollman PA (1992) SETTLE: An analytical version of the SHAKE and RATTLE algorithms for rigid water models. *J Comput Chem* 13(8):952–962.
68. Hess B (2008) P-LINCS: A parallel linear constraint solver for molecular simulation. *J Chem Theory Comput* 4(1):116–122.
69. Bussi G, Donadio D, Parrinello M (2007) Canonical sampling through velocity rescaling. *J Chem Phys* 126(1):014101.
70. Parrinello M, Rahman A (1981) Polymorphic transitions in single crystals: A new molecular dynamics method. *J Appl Phys* 52(12):7182–7190.
71. Keyes MH, Falley M, Lumry R (1971) Studies of heme proteins. II. Preparation and thermodynamic properties of sperm whale myoglobin. *J Am Chem Soc* 93(8):2035–2040.
72. Berendsen HJC, Postma JPM, DiNola A, Haak JR (1984) Molecular dynamics with coupling to an external bath. *J Chem Phys* 81(8):3684–3690.
73. Jongeward KA, et al. (1988) Picosecond and nanosecond geminate recombination of myoglobin with carbon monoxide, oxygen, nitric oxide and isocyanides. *J Am Chem Soc* 110(2):380–387.
74. Fischer H, Polikarpov I, Craievich AF (2004) Average protein density is a molecular-weight-dependent function. *Protein Sci* 13(10):2825–2828.